A Low-Power Low-Complexity Circuit for Event-Based Feature Extraction from sEMG

A Low-Power Low-Complexity Circuit for Event-Based Feature Extraction from sEMG

Andrea Prestia*, Andrea Mongardi, Danilo Demarchi, Fabio Rossi, Paolo Motto Ros
Department of Electronics and Telecommunications, Politecnico di Torino, Turin, Italy
*Corresponding author email: andrea.prestia@polito.it

***Abstract*—This paper presents an analog circuit for calibration-free event-driven myoelectric control of sEMG-based applications. The proposed solution is to be installed downstream of the conditioning chain of an sEMG sensor and consists of a Sallen-Key filter, acting as a differentiator in the main sEMG frequency band, and a voltage comparator. The output of the circuit is a quasi-digital signal, in which the muscle activity is mapped onto the time distribution of digital events. The design phase focused on noise robustness, and a prototype was tested during in-vivo experiments on both upper and lower limbs. Among the obtained results, besides a current consumption of only 12.92 µA, a median increase in the number of events of more than 25 % was achieved by varying the exerted muscle force in steps of 20 % MVC.**

***Index Terms*—Surface electromyography, Myoelectric control, Event-driven, Low-power, Bio-inspired electronics**

I. Introduction

The use of surface ElectroMyoGraphy (sEMG) to control Human-Machine Interfaces (HMIs) has grown significantly in recent decades, leading to increasingly compact solutions [1]–[4]. Major applications include post-stroke rehabilitation support [5], [6] and prosthetic control [7], [8], where sEMG is the most widely adopted biosignal for interpreting users' movements intentions, either alone or in combination with other non-invasive techniques through sensor fusion strategies [9], [10]. For these applications, full sEMG morphology information is often unnecessary, so signals are synthesized into simpler forms such as their envelope [11], [12], and the need for low-power low-latency wearable devices has paved the way for event-driven approaches such as neuromorphic edge computing [13] or level-crossing ADC-based acquisition systems [14]. On this front, our research group developed a wearable device for myoelectric control leveraging the event-based Average Threshold Crossing (ATC) technique, whose reference implementation and performance comparison with state-of-the-art sEMG sensors can be found in [15].

Essentially, ATC consists of hardware thresholding of the analog conditioned sEMG signal using a hysteresis voltage comparator, which generates the Threshold Crossing (TC) quasi-digital signal, whose information content lies in the time distance between the events generated each time the sEMG crosses the threshold. The threshold value, as implemented in [15], is not fixed but calibrated by the microcontroller of the sEMG sensor. Its embedded algorithm, while the subject holds the resting position for a few seconds, optimizes the threshold level against the environmental noise to trigger the generation of TC events only in the presence of muscle activation. The

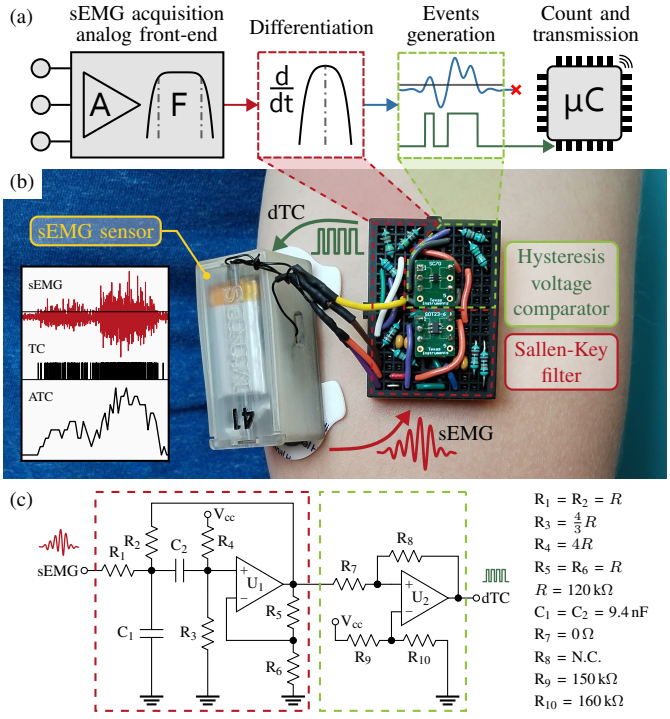

Fig. 1. (a) The circuit proposed in this work is to be installed downstream of the sEMG amplification and filtering chain, and the generated events can be counted and transmitted by the microcontroller used by the sEMG sensor [15]; (b) the developed prototype, with its two circuitry areas highlighted, positioned on a *biceps brachii*; (c) the circuit schematic and its components.

counting of events within time windows (e.g., 130 ms) results in the ATC feature, which showed a high correlation with the exerted muscle force [15]. Among its key applications, the ATC feature proved effective for both HMIs control using a custom-developed armband [16] and for Functional Electrical Stimulation (FES) modulation in rehabilitation scenarios [17].

In this work, to increase the versatility of the ATC technique and ease its adoption for standard acquisition and processing sEMG systems, we designed a low-power low-complexity circuit to enable sEMG-to-events conversion without the need for threshold calibration. Thus, this new implementation of ATC no longer requires either the presence of a DAC to generate the threshold or a dedicated algorithm executed by a microcontroller. The developed circuit, as shown in Fig. 1, is to be installed downstream of the sEMG-conditioning chain and comprises only a Sallen-Key filter and a voltage comparator.

All the experimental tests involving human subjects (healthy volunteers) have been authorized by the Comitato Bioetico di Ateneo of University of Turin, experimental code 445154.

II. Methods

The core idea is to apply a threshold to the derivative of the sEMG to generate events with respect to a variation in the signal from its previous state rather than in absolute terms as for standard ATC, with the main purpose of no longer needing a threshold calibration. As shown in Fig. 1, the designed circuit is made up of two stages: a Sallen-Key filter and a hysteresis voltage comparator. The first one has a two-fold role: first, to behave as a differentiator in the frequency range where most of the information content of the sEMG is, taking advantage of the transition band of a first-order high-pass filter, and second, to filter out the frequency components above the upper limit of the mentioned band. The two purposes can thus be achieved with just one second-order band-pass filter, with $Q = 0.707$, centered at a common cutoff frequency f_0. The second stage is then in charge of generating events by comparing the filter output with the threshold V_t using the hysteresis V_h. The generated events, after being counted within time windows, result in the differentiated ATC feature, henceforth referred to as dATC. We emphasize that the use of the proposed circuit is generalizable to any sEMG sensor as long as the design phase of the circuit is adapted to the device voltage dynamics.

Referring to Fig. 1-c, we selected the LPV821 [18] as U_1 and the TLV3691 [19] as U_2 for the Sallen-Key and voltage comparator, respectively, because of their low-power features, and the single-supply voltage V_{cc} was set to 1.8 V as in the main upstream conditioning circuit [15]. The design phase then focused on identifying the best (f_0, V_t, V_h) combination through LTspice® simulations with sEMG data as input, aiming for a noise-robust solution, thus choosing the values of resistors and capacitors to be used to build the prototype.

The sEMG data needed for the design phase were acquired from the *biceps brachii* of 3 volunteers using one of our sEMG sensors [15]. For each acquisition, each subject was asked to perform 5 elbow flexion repetitions, using a load equal to 70 % of the Maximal Voluntary Contraction (MVC) measured at the beginning of the experiment, alternating 10 s of contraction (holding the load with elbow at 90°) with 30 s of rest. Next, we artificially added white noise to the recorded sEMG data in order to obtain Signal-to-Noise Ratio (SNR) levels equal to 3 dB, 6 dB, 9 dB, and 12 dB; the resulting signals, as well as the original ones (whose average SNR is 19 dB), were used as input in the simulations. Considering that the sEMG signal bandwidth is up to 500 Hz with little energy contribution above 400 Hz [20] and dominant contribution in the 50 Hz–150 Hz range [21], the filter was tested in the condition of f_0 = 400 Hz, and f_0 = 200 Hz, to reduce the lower frequencies attenuation compared to f_0 = 400 Hz while preserving the differentiator behavior for the dominant band. Thus, a total of 30 simulations were run: 3 acquisitions × 5 SNR levels × 2 f_0 alternatives.

Each simulation output was finally processed in MATLAB®, where ATC and dATC features were computed and compared for each ATC window (i.e., 130 ms). To compute the ATC, the embedded threshold calibration algorithm of our sEMG sensor was reproduced, and its hysteresis value equal to 30 mV was set [15]. On the other hand, to extract the dATC feature, for which we recall no calibration but a fixed threshold is used, the 0.8 V–1 V range in 10 mV steps was explored for V_t, and the 20 mV–200 mV range in steps of 10 mV for V_h. We also added 17 mV as the lowest value of V_h because this is the internal hysteresis of the TLV3691 [19], which would allow resistors R_7 and R_8 not to be used (see Fig. 1-c).

To compare the dATC feature with ATC for each parameters combination, we defined an index of *Dynamics Increase* (DI), which corresponds to a three-dimensional matrix in which the rows and columns are V_t and V_h, respectively, and f_0 is the third dimension. Each element of DI is defined as in (1).

$$\begin{cases} DI_{f_0}(V_t, V_h) = median(\Delta_{f_0}(V_t, V_h)|_{load}) + \\ \qquad\qquad - \ median(\Delta_{f_0}(V_t, V_h)|_{rest}) \\ \Delta_{f_0}(V_t, V_h) = dATC_{f_0}(V_t, V_h) - ATC_{f_0}(V_t, V_h) \end{cases} \tag{1}$$

$DI_{f_0}(V_t, V_h)$ is rewarded if dATC is higher than ATC during the load phase, and penalized if dATC is higher than ATC while the subject is resting. Therefore, this scoring allowed us to evaluate which set of parameters results in the widest range of variation for dATC while dealing with noise robustness. To combine the outcomes among the different subjects, the DI matrices obtained from the three volunteers were summed together for each SNR level. Then, the resulting five matrices were further summed to each other by proportionally weighting their contribution, specifically by doubling the weight at each successive level (e.g., the matrix related to SNR equal to 9 dB is weighted twice more than the matrix related to 6 dB).

After the design phase was completed, a prototype featuring the best (f_0, V_t, V_h) combination previously identified was built, and one of our sEMG sensors was equipped with it (see Fig. 1-b). To count and transmit the number of generated events, in the same way as [15], the output of the circuit was connected to a free GPIO of the microcontroller whose firmware was modified to wireless transmit both the ATC and dATC features in order to compare them at the same time windows. The evaluation of the developed circuit was then carried out by acquiring ATC and dATC data from 5 additional volunteers while performing the same task described previously, but with three different load levels: 30 %, 50 %, and 70 % of the MVC measured at the beginning of the experiment, to test how dATC varies as the exerted muscle force changes. Moreover, to test whether this implementation could also be used for applications concerning lower limbs, such as the control of FES or exoskeletons for walking support, 3 subjects were asked to walk and run while recording data from the *gastrocnemius lateralis*. During these tests, threshold calibration for ATC was performed prior to the beginning of each acquisition.

III. Results and Discussion

The results of the design phase are reported in Fig. 2, showing the DI index as each circuit parameter varies in the

exploration space. The elements of the matrix are normalized according to the maximum and minimum values of DI obtained and the red circles indicate the best combination of V_t and V_h for the two different f_0 under investigation. Of course, to reduce the number of events due to noise and maximize those related to muscle activity, the closer V_t is to the signal baseline, the larger V_h must be used, and vice versa, as V_t increases, V_h should be lower. The best outcomes were achieved with f_0 = 200 Hz, V_t = 0.93 V, and V_h = 17 mV. On the other hand, if only the originally acquired signals, i.e., those not artificially corrupted by white noise, were taken into account, the combination of parameters with the highest DI would have been f_0 = 400 Hz, V_t = 0.91 V, and V_h = 17 mV, but the implementation would have been less robust to noise.

Following the prototype assembly (see Fig. 1) after the design phase, the current consumption of the developed circuit was measured using a DMM7510 multimeter [22]. The resulted value, equal to 12.92 µA, proves that the proposed circuit is a suitable equipment for low-power sensors, such as ours, whose total current consumption (including both analog and digital parts) is 480 µA when used in ATC mode [15].

The results of the in-vivo experiments are reported in Fig. 3. In particular, Fig. 3-a and 3-c refer to the tests carried out on 5 subjects performing elbow flexion movements at different percentage levels of MVC, while Fig. 3-b and 3-d refer to the walking and running tasks executed by 3 subjects. To generate the boxplots of Fig. 3-a and 3-b, all ATC windows related to muscle activity were considered, without distinction between subjects, and since both the dATC and ATC features were available for each window, they were ratioed (i.e., dATC/ATC) in order to investigate the dynamics of the new implementation compared to that of the calibrated one. On the other hand, the boxplots of Fig. 3-c and 3-d, in which the normalized dATC feature is reported, show how dATC varies according to the exerted muscle effort. The reason for normalization was to combine data belonging to different subjects, and it was computed by dividing, for each subject, the dATC values by the median value resulted from the task at higher effort (i.e., 70 % MVC for Fig. 3-c, and running for 3-d). No boxplots related to the ATC windows under resting conditions were reported because both the ATC and dATC features, thanks to their noise robustness, did not exhibit activations (i.e., their values were zeros) while subjects were not moving.

As can be seen from Fig. 3-a and 3-b, dATC is typically greater than ATC, thus allowing for better resolution in identifying muscle activity. Specifically, the medians of boxplots in Fig. 3-a are 1, 1.13, and 1.21 for 30 %, 50 %, and 70 % MVC respectively, while the medians of boxplots in 3-b are 1.44 and 1.2 for walking and running exercises. Actually, this increase in dynamics has not always a positive effect. In fact, since during walking the dynamics of dATC was greater than that of ATC more than during running, this results in a smaller difference between the two tasks, thus moving the medians of the boxplots of Fig. 3-d closer together. In the case of ATC, the lower number of events detected during walking, whose median value is 0.62, would indeed facilitate its discrimination

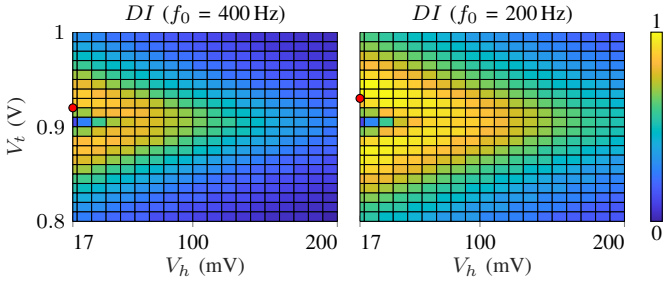

Fig. 2. Normalized DI matrix resulted from the design phase. The red circles indicate the best combination of V_t and V_h for each f_0.

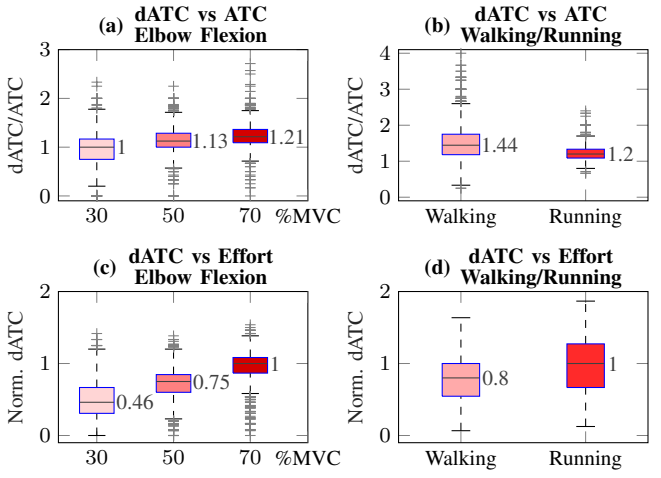

Fig. 3. In-vivo experimental phase results. In (a), the ratio between dATC and ATC for each ATC window in load condition during elbow flexion movements is summarized, while the behavior of dATC as the muscle effort increases is reported in (c). In (b) and (d), parallel to (a) and (c) respectively, the obtained results during walking and running tasks are reported.

from running. Nevertheless, both Fig. 3-c and 3-d boxplots show an increasing trend of activity as load increases. In particular, the results obtained in the case of elbow flexion show how the normalized median increase of dATC is equal to 29 % when the load varies from 30 % to 50 % MVC, and to 25 % when varying from 50 % to 70 % MVC.

IV. Conclusion

In this paper we presented a low-complexity analog circuit for sEMG-to-events conversion, which does not require calibration routines and could be adopted by any sEMG sensor for which full sEMG morphology is not required and low-power features are prioritized.

Compared to our previous event-based technique, whose usability for the control of HMIs or FES has been already validated, this new implementation showed wider dynamics, e.g., when performing elbow flexion at 70 % MVC loading conditions, the number of detected events was 21 % higher.

The preliminary outcomes described in this paper are positive and encouraging, and the next step will be to test this implementation for the above-mentioned applications such as hand gestures recognition and FES modulation.

REFERENCES

[1] D. Xiong, D. Zhang, Y. Chu, Y. Zhao, and X. Zhao, "Intuitive human-robot-environment interaction with EMG signals: A review," *IEEE/CAA Journal of Automatica Sinica*, vol. 11, no. 5, pp. 1075–1091, 2024.

[2] M. Zheng, M. S. Crouch, and M. S. Eggleston, "Surface electromyography as a natural human–machine interface: A review," *IEEE Sensors Journal*, vol. 22, no. 10, pp. 9198–9214, 2022.

[3] Z. Zheng, Z. Wu, R. Zhao, Y. Ni, X. Jing, and S. Gao, "A review of EMG-, FMG-, and EIT-based biosensors and relevant human-machine interactivities and biomedical applications," *Biosensors*, vol. 12, no. 7, 2022.

[4] H. Lee, S. Lee, J. Kim, H. Jung, K. J. Yoon, S. Gandla, H. Park, and S. Kim, "Stretchable array electromyography sensor with graph neural network for static and dynamic gestures recognition system," *npj Flexible Electronics*, vol. 7, no. 1, p. 20, 2023.

[5] L. Zongxing, Z. Jie, Y. Ligang, C. Jinshui, and L. Hongbin, "The human–machine interaction methods and strategies for upper and lower extremity rehabilitation robots: A review," *IEEE Sensors Journal*, vol. 24, no. 9, pp. 13 773–13 787, 2024.

[6] H. Yang, J. Wan, Y. Jin, X. Yu, and Y. Fang, "EEG- and EMG-driven poststroke rehabilitation: A review," *IEEE Sensors Journal*, vol. 22, no. 24, pp. 23 649–23 660, 2022.

[7] V. Mendez, F. Iberite, S. Shokur, and S. Micera, "Current solutions and future trends for robotic prosthetic hands," *Annual Review of Control, Robotics, and Autonomous Systems*, vol. 4, pp. 595–627, 2021.

[8] C. Ahmadizadeh, M. Khoshnam, and C. Menon, "Human machine interfaces in upper-limb prosthesis control: A survey of techniques for preprocessing and processing of biosignals," *IEEE Signal Processing Magazine*, vol. 38, no. 4, pp. 12–22, 2021.

[9] C. Brambilla, I. Pirovano, R. M. Mira, G. Rizzo, A. Scano, and A. Mastropietro, "Combined use of EMG and EEG techniques for neuromotor assessment in rehabilitative applications: A systematic review," *Sensors*, vol. 21, no. 21, 2021.

[10] H. Zhou and G. Alici, "Non-invasive human-machine interface (HMI) systems with hybrid on-body sensors for controlling upper-limb prosthesis: A review," *IEEE Sensors Journal*, vol. 22, no. 11, pp. 10 292–10 307, 2022.

[11] M. Kalbasi, M. Shaeri, V. A. Mendez, S. Shokur, S. Micera, and M. Shoaran, "A hardware-efficient EMG decoder with an attractor-based neural network for next-generation hand prostheses," *arXiv preprint arXiv:2405.20052*, 2024.

[12] G. Yu, Z. Deng, Z. Bao, Y. Zhang, and B. He, "Gesture classification in electromyography signals for real-time prosthetic hand control using a convolutional neural network-enhanced channel attention model," *Bioengineering*, vol. 10, no. 11, p. 1324, 2023.

[13] A. Vitale, E. Donati, R. Germann, and M. Magno, "Neuromorphic edge computing for biomedical applications: Gesture classification using EMG signals," *IEEE Sensors Journal*, vol. 22, no. 20, pp. 19 490–19 499, 2022.

[14] Y. Zhao and Y. Lian, "Event-driven circuits and systems: A promising low power technique for intelligent sensors in AIoT era," *IEEE Transactions on Circuits and Systems II: Express Briefs*, vol. 69, no. 7, pp. 3122–3128, 2022.

[15] F. Rossi, A. Mongardi, P. Motto Ros, M. Ruo Roch, M. Martina, and D. Demarchi, "Tutorial: A versatile bio-inspired system for processing and transmission of muscular information," *IEEE Sensors Journal*, vol. 21, no. 20, pp. 22 285–22 303, 2021.

[16] A. Mongardi, F. Rossi, A. Prestia, P. Motto Ros, M. Ruo Roch, M. Martina, and D. Demarchi, "Hand gestures recognition for human-machine interfaces: A low-power bio-inspired armband," *IEEE Transactions on Biomedical Circuits and Systems*, vol. 16, no. 6, pp. 1348–1365, 2022.

[17] A. Prestia, F. Rossi, A. Mongardi, P. Motto Ros, M. Ruo Roch, M. Martina, and D. Demarchi, "Motion analysis for experimental evaluation of an event-driven FES system," *IEEE Transactions on Biomedical Circuits and Systems*, vol. 16, no. 1, pp. 3–14, 2022.

[18] Texas Instruments. LPV821. Accessed: October 6, 2024. [Online]. Available: https://www.ti.com/product/LPV821

[19] Texas Instruments. TLV3691. Accessed: October 6, 2024. [Online]. Available: https://www.ti.com/product/TLV3691

[20] G. De Luca, *Fundamental Concepts in EMG Signal Acquisition*. DelSys Incorporated, 2003.

[21] C. J. De Luca, *Surface Electromyography: Detection and Recording*. DelSys Incorporated, 2002.

[22] Tektronix. Keithley DMM7510 7.5 digit graphical sampling multimeter. Accessed: October 6, 2024. [Online]. Available: https://www.tek.com/en/products/keithley/digital-multimeter/dmm7510